Compensating Fiber Gratings for Source Flatness to Reduce Multiple-Access Interferences in Optical CDMA Network Coder/Decoders

Jen-Fa Huang, Chen-Mu Tsai, and Yu-Lung Lo

***Abstract*—A fiber-Bragg-grating (FBG)-based optical code-division multiple-access (OCDMA) network coder/decoder (codec) is investigated for its interference suppression induced by nonflattened broad-band lightwave sources. Since each network user with different signature address code has different spectral distribution, the nonflattened light sources will cause multiple-access interference (MAI). Flatness compensation schemes are proposed to solve the MAI effects induced by nonflattened broad-band light sources. By arranging the same coding scheme but in different spectral coding band, spectral chips from FBG coder/compensator will incoherently power summed in the photodetectors to approach a more flattened power level. Signal-to-interference ratio (SIR) performances are evaluated with such compensation method for the discussed OCDMA network.**

***Index Terms*—Fiber Bragg grating (FBG), fiber-optic code-division multiple-access (FO-CDMA), multiple-access interference (MAI), pseudoorthogonal code.**

I. Introduction

FIBER-OPTIC code-division multiple-access (FO-CDMA) is a technique that allows multiple users in local area networks (LANs) to access the same fiber channel asynchronously without delay or scheduling. Several methods have been proposed to achieve passive optical CDMA. Chief among these are systems making use of optical delay lines and optical orthogonal codes for time-domain coding of CDMA, and modified optical CDMA systems employing spectral coding through diffraction gratings, confocal lenses, and phase/amplitude masks [1]. Compared with these, fiber Bragg gratings (FBGs) are more convenient for inscription of the spectral codes necessary for optical CDMA applications and have proven useful in many CDMA systems [2]–[5].

Multiple-access interference (MAI) has been shown to limit performance of optical CDMA networks that perform correlation decoding on the basis of received optical power. In order to reduce undesirable MAI effects, Huang *et al.* [6], [7] and Zou *et al.* [8] configured FBG coder/decoders (codecs) on the basis of spectral amplitude coding (SAC). SAC systems employ broad-band sources to get spectral coding chips. Unfortunately, the spectra produced by contemporary broad-band sources are not flat and produce spectrally coded chips with nonequal power levels. The resulting imbalanced chip power distribution at the coder output causes MAI problems at the receiver.

The standard approach to countering MAI effects caused by nonflattened optical sources is some form of equalization of the incoherent broad-band source. For example, Baran *et al.* [9] used acoustooptical tunable filters to equalize spectral segments. Schiffer *et al.* [10] applied an integrated planar optical circuit to develop a smart dynamic wavelength equalizer. These equalization schemes provide a flat spectrum but do not increase the bandwidth from which to slice chips, and so cannot offer an increased number of coding chips. To promote spectrum efficiency, Nguyen *et al.* [11] demonstrated tuning the chip bandwidth to achieve equal power among spectral chips, which he achieved by use of diffraction gratings, confocal lenses, and amplitude masks. Alternative to Nguyen's methodology, FBG filters can also be used to achieve equal power among spectral chips, but such special FBGs are not easily fabricated.

The conventional source equalization techniques all work within or adjacent to the broad-band light source itself, thereby supplying equalized broad-band light to the optical network. Nguyen's system, however, used an unequalized broad-band light source and instead made complex modifications to both encoder and decoder. This paper uses a novel method called source flatness compensation (SFC). The proposed methodology is similar to Nguyen's in that it works with unflattened light and provides power compensation at the codec levels. SFC avoids Nguyen's complex hardware, and also the expense of custom FBG design. In SFC, common ITU-standard FBGs are employed, one for each FBG of each coder and decoder, while a conventional broad-band source supplies unflattened light to the network. These FBGs equalize the chip power by adding power to the lower power chips. This additional power comes from the "skirt area" power of the source, power that is unused in traditional methods. As with Nguyen's method, SFC has the additional theoretical value of allowing chips to be sliced from a wider band of the original source spectrum, thereby permitting an increased number of chips.

The remainder of this paper is organized as follows. In Section II, source flatness effects in nearly orthogonal M-sequence codes on spectrally pseudoorthogonal fiber Bragg gratings are described. In Section III, FBG encoder/compensator pairs and decompensator/decoder pairs are presented. Examples are given in Section IV to clarify the operation of the proposed

Manuscript received January 31, 2003; revised December 4, 2003. This work was supported by the Ministry of Education Program for Promoting Academic Excellence of Universities under Grant A-91-E-FA08-1-4 and in part by the National Science Council under Grant NSC 92-2622-6-011-001.

J.-F. Huang and C.-M. Tsai are with the Department of Electrical Engineering, National Cheng Kung University, Taiwan, R.O.C. (e-mail: huajf@ee.ncku.edu.tw).

Y.-L. Lo is with the Department of Mechanical Engineering, National Cheng Kung University, Taiwan, R.O.C. (e-mail: loyl@mail.ncku.edu.tw).

Digital Object Identifier 10.1109/JLT.2004.824551

0733-8724/04$20.00 © 2004 IEEE

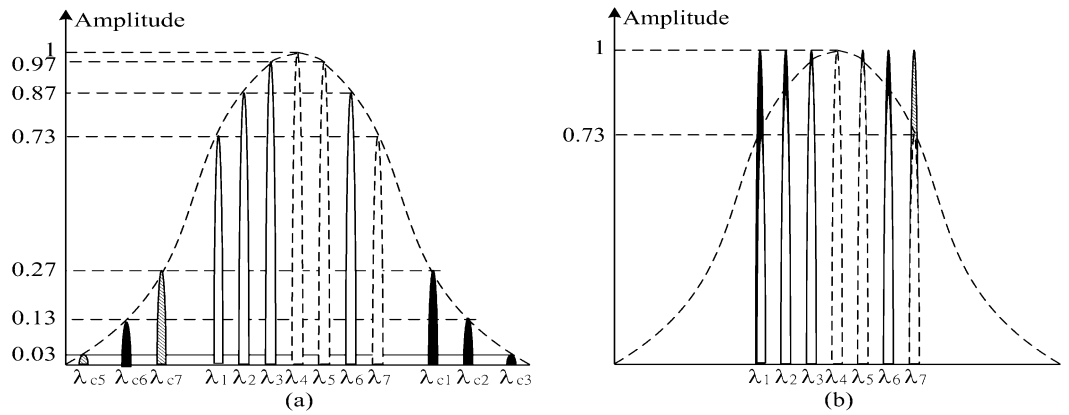

Fig. 1. Broad-band source power spectral profile: (a) chips without compensation (Gaussian profile) and (b) chips after flatness compensation.

SFC process. Section V evaluates performance of the proposed method in terms of signal-to-interference ratio (caused by source nonflattened profile) for noncompensated and compensated cases. Conclusions are presented in Section VI.

II. Source Flatness Effects on FO-CDMA

When a spectrally perfect FO-CDMA system is considered, chip energies among the coded spectral chips are all equal. Under such conditions, different system users do not interfere with each other. In practical CDMA systems, however, source spectral power distribution is not flat in the coding area. This nonflatness deeply influences system performance by creating different chip power allocations for different users, which in turn causes MAI.

In general, the spectral profile of a broad-band light sources approaches a Gaussian profile and can be expressed as

$$L(\lambda) = \exp\left[\frac{-(\lambda-\lambda_c)^2}{2\sigma_s^2}\right] \tag{1}$$

where λ_c and σ_s are, respectively, the central wavelength and the bandwidth of the broad-band sources. Similarly, when flattened broad-band light is reflected from a FBG, the spectral profile of the reflected light also approaches a Gaussian profile, expressed here as

$$Z(\lambda) = \exp\left[\frac{-(\lambda-\lambda_i)^2}{2\sigma_F^2}\right] \tag{2}$$

where λ_i and σ_F are, respectively, the central wavelength and the spectral chip width (FWHM$=$ 0.2–0.3 nm) of the FBG filters.

Upon incidence of a broad-band source's Gaussian signal $L(\lambda)$ (1) on an FBG coding device characterized by (2), the spectral shape z_i of the reflected chip can also be assumed to be Gaussian. The chip power z_i for each reflected chip pulse can be obtained as

$$z_i = \int_{\lambda_i-\Delta B/2}^{\lambda_i+\Delta B/2} \exp\left[\frac{-(\lambda-\lambda_c)^2}{2\sigma_s^2} - \frac{(\lambda-\lambda_i)^2}{2\sigma_F^2}\right] d\lambda \tag{3}$$

where ΔB is the bandwidth of the FBG filter as measured at the first zeros.

Fig. 1 depicts a broad-band source power spectral profile with the spectral profiles of a set of chips both without flatness compensation and after flatness compensation (the figure is highly exaggerated for purposes of illustration). Clearly, the uncompensated Gaussian spectrum shows a strong but nonflat profile in the central region and rolls off at both right and left skirts, as illustrated in Fig. 1(a). But when the skirt peaks are added to those in the central region, a greatly flattened spectrum results, as can be seen in Fig. 1(b). With this goal in mind, the cascaded FBG transmitters in the proposed FO-CDMA network codec are configured with both encoders and compensators. At the receiving end, the FBG modules contain both decoders and decompensators.

The frequency pattern of spectral chips centered around the grating frequencies is determined by the pseudoorthogonal codes written in the FBGs. Pseudoorthogonal codes having good correlation properties (i.e., high autocorrelation peaks with low sidelobes and low cross-correlation functions) are needed to reduce undesired interference from other simultaneous system users. Binary linear codes such as the maximal-length sequence (M-sequence) codes and Walsh–Hadamard codes possess the above-mentioned pseudoorthogonality and are useful for incoherent optical CDMA networks. Nearly orthogonal M-sequence codes will be used in this paper. The following discussion of M-sequences and correlation properties in a balanced receiver follow the work in [12].

Denote $\mathbf{X} = (x_1, x_2, \ldots, x_N)$ and $\mathbf{Y} = (y_1, y_2, \ldots, y_N)$ as two M-sequence code vectors of period N. The periodic correlation between $\mathbf{X}$ and $\mathbf{Y}$ is defined as $R_{\mathbf{XY}}(n) = \sum_{i=1}^{N} x_i y_{i+n}$, where the subscript $i+n$ is taken modulo N. In the proposed FO-CDMA system, M-sequence code vectors $\mathbf{Y} = T^n\mathbf{X}$ are assigned to different network users, where T^n is an operator that shifts code vectors $\mathbf{X}$ cyclically to the right by n bits, $0 \le n \le N-1$. According to the characteristic shift-and-add property of M-sequence code, the correlation function is obtained as follows:

$$R_{\mathbf{XY}}(n) = \begin{cases} \frac{(N+1)}{2}, & \text{for } n = 0; \\ \frac{(N+1)}{4}, & \text{for } n = 1 \text{ to } N-1. \end{cases} \tag{4}$$

Note that for $n = 0$, $\mathbf{X}$ and $\mathbf{Y}$ are the same code vector and $R_{\mathbf{XY}}(n)$ corresponds to the autocorrelation of $\mathbf{X}$ (or $\mathbf{Y}$). For

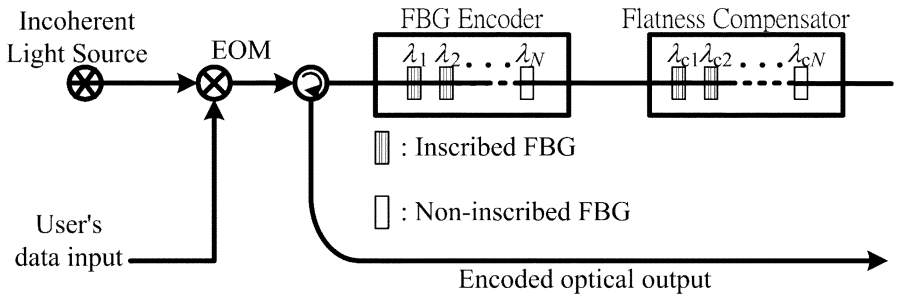

Fig. 2. Configuration of FBG-based OCDMA coder/compensator.

$n = 1$ to $N-1$, $\mathbf{X}$ and $\mathbf{Y}$ are different code vectors and $R_{\mathbf{XY}}(n)$ corresponds to the cross-correlation between $\mathbf{X}$ and $\mathbf{Y}$.

Let $\bar{\mathbf{X}} = (\bar{x}_1, \bar{x}_2, \ldots, \bar{x}_N)$ be the complement of $\mathbf{X}$ with chip elements obtained by $\bar{x}_i = 1 - x$. The periodic correlation between $\bar{\mathbf{X}}$ and $\mathbf{Y}$ then is $R_{\bar{\mathbf{X}}\mathbf{Y}}(n) = \sum_{i=1}^{N} \bar{x}_i y_{i+n}$. In the discussed FO-CDMA system, the receiver that computes correlation difference $R_{\mathbf{XY}}(n) - R_{\bar{\mathbf{X}}\mathbf{Y}}(n)$ will result in (5) as shown at the bottom of the page.

With respect to the above equation, a receiver decoder in the FO-CDMA network can be suitably designed using FBGs.

Since pseudoorthogonal M-sequence codes can achieve $R_{\mathbf{XY}}(n) - R_{\bar{\mathbf{X}}\mathbf{Y}}(n) = 0$, the address code vector $\mathbf{X}$ is used to construct two decoder branches based on $\mathbf{X}$ and $\bar{\mathbf{X}}$ in the receiver. The receiver user $\mathbf{X}$ that computes the correlation subtraction $R_{\mathbf{XY}}(n) - R_{\bar{\mathbf{X}}\mathbf{Y}}(n)$ will then receive a null value. That is, an intended receiver user $\mathbf{X}$ with decoder design based on the calculation of $R_{\mathbf{XY}}(n) - R_{\bar{\mathbf{X}}\mathbf{Y}}(n)$ will reject the signal coming from the interfering user having sequence $\mathbf{Y} = T^n\mathbf{X}$, $n \neq 0$. Hence, by assigning N cycle shifts of a single M-sequence to N users, there exists an optical network that can theoretically support N simultaneous users without any interference. Quasiorthogonality, therefore, has been obtained between the FO-CDMA network users.

III. Fiber-Grating Optical CDMA Coders/Compensators

To reduce MAI due to nonflattened source spectrum, the FBG-coder can be cascaded with a flatness compensator in the transmitter, and the FBG-decoder can be preceded with a flatness decompensator in the receiver. Figs. 2 and 3 depict this conceptual arrangement as the proposed SFC fiber-optic CDMA coder/compensator and decompensator/decoder in terms of cascaded multiple FBG devices.

Fig. 2 illustrates the transmitter configuration of the FO-CDMA network system. The transmitter encoder module consists of a series of FBGs, an intensity E/O modulator, and an incoherent broad-band optical source. Each bit of information from the kth user is ON–OFF shift keying the broad-band incoherent optical carrier to fulfill electrical/optical modulation. The modulated optical field corresponding to each data bit is then directed to an FBG coder/compensator for the spectral encoding operation. The spectrum-encoded lightwave signals of each transmitter are then put together with a star coupler and broadcast to all receivers in the network.

In the receiver end of the FO-CDMA network, the received signal spectrum is a sum of all of the active users' transmitted signal spectra $\mathbf{S}(\lambda) = \sum_{k=1}^{N} b_k \mathbf{X}_k(\lambda - l_k)$, where b_k is the kth user's information bit and l_k is the kth user's arbitrary shift in the spectral domain. The receiver applies a correlating decoder to the incoming signal to extract the desired bit stream. The kth correlator output $\int_{-\infty}^{\infty} \mathbf{S}(\lambda)\mathbf{X}_k(\lambda)d\lambda$ consists of the desired data stream for the kth user and the MAI coming from the other users. Note that the decision device in the receiver decoder sums the power of the incoming chips to determine the information data bit.

Fig. 3 illustrates the receiver configuration of an FO-CDMA network system. Flatness decompensator and multiple-access decoder are cascaded to extract the corresponding compensating and coding-chips. For the timing of grating path alignment, the decompensator/decoder modules are configured with complementary correlation-decoding branches corresponding to signature codes $\mathbf{X}_k(\lambda)$ and $\bar{\mathbf{X}}_k(\lambda)$, respectively. In the upper branch, the received signal $\mathbf{S}(\lambda)$ enters into the FBG decompensator/decoder corresponding to signature code $\mathbf{X}_k(\lambda)$ and is reflected with signal energy $R_{\mathbf{SX}_k}$. In the lower branch, the received signal $\mathbf{S}(\lambda)$ enters into the complementary decompensator/decoder corresponding to signature code $\bar{\mathbf{X}}_k(\lambda)$ and is reflected with signal energy $R_{\mathbf{S}\bar{\mathbf{X}}k}$. The subtraction of $R_{\mathbf{SX}_k} - R_{\mathbf{S}\bar{\mathbf{X}}k}$ is then implemented in the balanced detector to retrieve the desired data bitstream.

$$
\begin{aligned}
R_{\mathbf{XY}}(n) - R_{\bar{\mathbf{X}}\mathbf{Y}}(n) &= \left[\sum_{i=1}^{N} X_i X_{i+n}\right] - \left[\sum_{i=1}^{N} (1 - X_i) X_{i+n}\right] \\
&= 2R_{\mathbf{XY}}(n) - R_{\mathbf{XY}}(0) \\
&= \begin{cases} \frac{(N+1)}{2}, & \text{for ``matched'' codes pair } (\mathbf{Y} = \mathbf{X}) \\ \frac{2(N+1)}{4} - \frac{(N+1)}{2} = 0, & \text{for ``unmatched'' codes } (\mathbf{Y} \neq \mathbf{X}). \end{cases}
\end{aligned} \tag{5}
$$

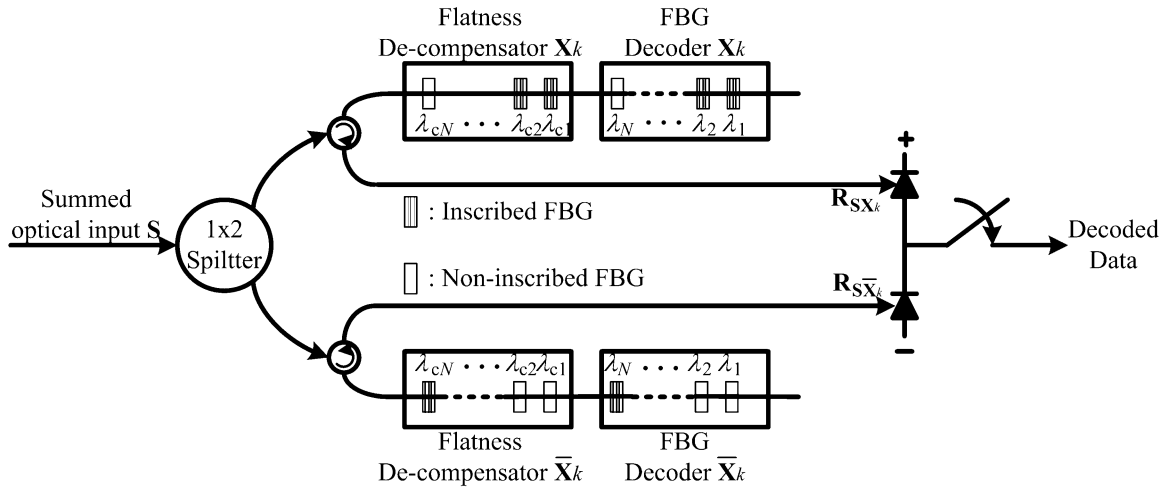

Fig. 3. Configuration of FBG-based OCDMA decompensator/decoder.

TABLE I
COMPENSATIVE SEVEN-CHIP SPECTRA IN THE TRANSMITTER

	assigned address sequence	Data bit	coding chips							compensating chips					
			λ_1	λ_2	λ_3	λ_4	λ_5	λ_6	λ_7	λ_{c1}	λ_{c2}	λ_{c3}	λ_{c5}	λ_{c6}	λ_{c7}
User #1	1 1 1 0 0 1 0	1	0.73	0.87	0.97	0	0	0.87	0	0.27	0.13	0.03	0	0.13	0
User #2	0 1 1 1 0 0 1	0	0	0	0	0	0	0	0	0	0	0	0	0	0
User #3	1 0 1 1 1 0 0	1	0.73	0	0.97	1	0.97	0	0	0.27	0	0.03	0.03	0	0
User #4	0 1 0 1 1 1 0	1	0	0.87	0	1	0.97	0.87	0	0	0.13	0	0.03	0.13	0
User #5	0 0 1 0 1 1 1	1	0	0	0.97	0	0.97	0.87	0.73	0	0	0.03	0.03	0.13	0.27
User #6	1 0 0 1 0 1 1	0	0	0	0	0	0	0	0	0	0	0	0	0	0
User #7	1 1 0 0 1 0 1	1	0.73	0.87	0	0	0.97	0	0.73	0.27	0.13	0	0.03	0	0.27
Summed signal **S**			2.19	2.61	2.91	2	3.88	2.61	1.46	0.81	0.39	0.09	0.12	0.39	0.54

IV. EXAMPLE CHIPS POWER COMPENSATION

For ease of modular design, the coder and compensator chips are arranged with the same coding scheme but with different spectral coding bands. With coded fiber gratings of chips length N, the FBG-coder chips' power with wavelengths $(\lambda_1, \lambda_2, \ldots, \lambda_N)$ is compensated by those FBG-compensator chips power with wavelengths $(\lambda_{c1}, \lambda_{c2}, \ldots, \lambda_{cN})$. In other words, the compensator chip wavelength λ_{c1} is paired to the coder chip wavelength λ_1 for chip power compensation. Other wavelength pairs $(\lambda_2, \lambda_{c2})$, $(\lambda_3, \lambda_{c3})$, etc., are similarly placed for the respective chips power compensation.

Table I presents an example to illustrate the coding/compensating processes, while Tables II and III illustrate decompensating/decoding processes, with M-sequence coded fiber gratings of length $N = 7$ (refer to Fig. 1). The example assumes a simple network composed of seven senders, each with a unique address code. Two receivers will be considered, one with the code of user #1 (designated receiver #1) and one with the code of user #2 (designated receiver #2). As can be seen in Table I, users #2 and #6 are assumed to transmit logical "0," while the other users transmit logical "1." Thus, user #1 is sending logical "1" with the signature $\mathbf{X}_1 = (1,1,1,0,0,1,0)$, which after the FBG-coder is composed of wavelengths $(\lambda_1, \lambda_2, \lambda_3, \lambda_6)$ in the central region of the Gaussian source spectrum, and after the FBG-compensator includes wavelengths $(\lambda_{c1}, \lambda_{c2}, \lambda_{c3}, \lambda_{c6})$ from the Gaussian skirt. Other users are similarly given coding and compensating wavelengths according to their assigned FBG codes.

TABLE II
COMPENSATING SEVEN-CHIP SPECTRA IN THE RECEIVER FOR USER #1, WITH SIGNATURE $\mathbf{X}_1 = (1,1,1,0,0,1,0)$

Summed Signal **S**	Received coding spectra							Received compensating spectra						
	λ_1	λ_2	λ_3	λ_4	λ_5	λ_6	λ_7	λ_{c1}	λ_{c2}	λ_{c3}	λ_{c4}	λ_{c5}	λ_{c6}	λ_{c7}
	2.19	2.61	2.91	2	3.88	2.61	1.46	0.81	0.39	0.09	0	0.12	0.39	0.54
Signature X_1	1	1	1	0	0	1	0	1	1	1	0	0	1	0
Correlation Rs_{X_1}	2.19	2.61	2.91	0	0	2.61	0	0.81	0.39	0.09	0	0	0.39	0
	2.19+2.61+2.91+2.61=10.32							0.81+0.39+0.09+0.39=1.68						
	10.32+1.68=12 units power													
Signature $\overline{X}_1$	0	0	0	1	1	0	1	0	0	0	1	1	0	1
Correlation $Rs_{\overline{X}_1}$	0	0	0	2	3.88	0	1.46	0	0	0	0	0.12	0	0.54
	2+3.88+1.46=7.34							0.12+0.54=0.66						
	7.34+0.66=8 units power													

TABLE III
COMPENSATIVE SEVEN-CHIP SPECTRA IN THE RECEIVER FOR USER #2, WITH SIGNATURE $\mathbf{X}_2 = (0,1,1,1,0,0,1)$

Summed Signal **S**	Received coding spectra							Received compensating spectra						
	λ_1	λ_2	λ_3	λ_4	λ_5	λ_6	λ_7	λ_{c1}	λ_{c2}	λ_{c3}	λ_{c4}	λ_{c5}	λ_{c6}	λ_{c7}
	2.19	2.61	2.91	2	3.88	2.61	1.46	0.81	0.39	0.09	0	0.12	0.39	0.54
Signature X_2	0	1	1	1	0	0	1	0	1	1	1	0	0	1
Correlation Rs_{X_2}	0	2.61	2.91	2	0	0	1.46	0	0.39	0.09	0	0	0	0.54
	2.61+2.91+2+1.46=8.98							0.39+0.09+0.54=1.02						
	8.98+1.02=10 units power													
Signature $\overline{X}_2$	1	0	0	0	1	1	0	1	0	0	0	1	1	0
Correlation $Rs_{\overline{X}_2}$	2.19	0	0	0	3.88	2.61	0	0.81	0	0	0	0.12	0.39	0
	2.19+3.88+2.61=8.68							0.81+0.12+0.39=1.32						
	8.68+1.32=10 units power													

After optical data coding in the FBG coders/compensators, the coded spectral chips are combined (summed signal $\mathbf{S}$ in Table I) and broadcast to each receiver in the network. Each receiver receives the resultant code vector $\mathbf{S} = [\mathbf{S}_{\rm cod}, \mathbf{S}_{\rm com}]$, with $\mathbf{S}_{\rm cod} = (2.19, 2.61, 2.91, 2, 3.88, 2.61, 1.46)$ and $\mathbf{S}_{\rm com} = (0.81, 0.39, 0.09, 0, 0.12, 0.39, 0.54)$ being subvectors of the multiple-access coders and flatness compensators, where the subscripts "cod" and "com" stand, respectively, for "coding" and "compensating." These subvectors are the power sum obtained by adding together the spectral chips from the FBG coder/compensator corresponding to every active user.

In order to spectrally decode the kth user's information data, the received signal vector $\mathbf{S} = [\mathbf{S}_{\rm cod}, \mathbf{S}_{\rm com}]$ is used to multiply the decoder/decompensator signature functions $\mathbf{X}_k$ and $\bar{\mathbf{X}}_k$ for correlation operations. Table II shows the spectral chip sequences contributed by the flatness decompensator and the multiple-access decoder for receiver #1, with signature $\mathbf{X}_1 = (1, 1, 1, 0, 0, 1, 0)$. The upper branch chips' vector contributed by the FBG-decoder is $\mathbf{S}_{\rm cod}\mathbf{X}_1 = (2.19, 2.61, 2.91, 0, 0, 2.61, 0)$, and that contributed by the decompensator is $\mathbf{S}_{\rm com}\mathbf{X}_1 = (0.81, 0.39, 0.09, 0, 0, 0.39, 0)$. The spectral chips reflected from the decoder/decompensator $\mathbf{X}_1$ are $R_{\mathbf{SX}_1} = |\mathbf{SX}_1| = |\mathbf{S}_{\rm cod}\mathbf{X}_1| + |\mathbf{S}_{\rm com}\mathbf{X}_1| = 12$ units of spectral power in the upper photodiode of the balanced detector.

In the complementary portion of Table II, the lower branch chips' vector contributed by the complementary decoder is $\mathbf{S}_{\rm cod}\bar{\mathbf{X}}_1 = (0, 0, 0, 2, 3.88, 0, 1.46)$, and that contributed by the complementary decompensator is $\mathbf{S}_{\rm com}\bar{\mathbf{X}}_1 = (0, 0, 0, 0, 0.12, 0, 0.54)$. The spectral chips from the complementary decoder/decompensator $\bar{\mathbf{X}}_1$ are $R_{\mathbf{S}\bar{\mathbf{X}}_1} = |\mathbf{S}\bar{\mathbf{X}}_1| = |\mathbf{S}_{\rm cod}\bar{\mathbf{X}}_1| + |\mathbf{S}_{\rm com}\bar{\mathbf{X}}_1| = 8$ units of spectral power in the lower photodiode of the balanced detector. The balanced detector constructed with the above upper and lower photodiodes therefore results in $R_{\mathbf{SX}_1} - R_{\mathbf{S}\bar{\mathbf{X}}_1} = 4$ units of photocurrent, corresponding to a detected logical "1" data bit for the first receiver user.

Following the discussion above, correlation-decoding processes for receiver #2 are similarly implemented. Table III shows the spectral chip sequences contributed by the flatness decompensator and the multiple-access decoder for receiver #2 with signature $\mathbf{X}_2 = (0, 1, 1, 1, 0, 0, 1)$. While the main coding chips are distributed in the central Gaussian region, the Gaussian skirts area is reserved for compensating chips to compensate for the insufficient power of the main coding chips.

Application of the same technique will yield correlation-decoding processes for all additional users and receivers.

V. Evaluation of Source Flatness Compensation

Signal-to-interference ratio (SIR) is an important parameter for studying the flatness effect of Gaussian sources in an FO-CDMA network. For an M-sequence code $(x_1, x_2, \ldots, x_N)$ of length N and spectral energy z_i for the reflected chips, SIR can be expressed [12] in the form

$$\text{SIR} = \frac{\left(\sum_{i=1}^{N} x_i^2 z_i\right)^2}{\sum_{k=1}^{K}\left(\sum_{i=1}^{N} x_i x_{i+k} z_i - \sum_{i=1}^{N} \bar{x}_i x_{i+k} z_i\right)^2}. \tag{6}$$

The numerator is the desired optical signal power in a bit period and the denominator is the MAI power from $K-1$ interfering users, with K being the number of active users. The possible number of active users under a specified SIR value can then be estimated. Here, only multiple-access noise effects caused by nonflattened light source spectra are considered.

In (6), the signal term $\sum_{i=1}^{N} x_i^2 z_i$ accounts for the fact that the signal at the positive photodiode undergoes two reflections from the FBGs (once in the encoder and once in the decoder). Similar deductions can be made for the two terms in the interference. The terms

$$I_U^k = \sum_{i=1}^{N} x_i x_{i+k} z_i \tag{7}$$

and

$$I_L^k = \sum_{i=1}^{N} \bar{x}_i x_{i+k} z_i \tag{8}$$

denote the mean intensities received on the positively and negatively biased photodiodes for interfering user k. Using Gaussian statistics for the decision variable resulting from integration of the balanced photodetector output, the subtraction $I_U^k - I_L^k$ becomes zero in the case of perfect cancellation of interfering signals.

The mean intensity functions I_U^k and I_L^k and of (7) and (8) are dependent on the code distribution. Different code sequences have different code distributions and hence different coded amplitudes of spectral chips. For example, the M-sequence (0, 1, 0, 1, 1, 1, 0) has the most concentrated chip distribution. The reflecting and transmitting power in the matched signature decoder is larger than the other signature decoders. This is due to increasing intensity of broad-band light sources toward the center wavelength. On the contrary, the chip distribution of code sequence (1, 1, 0, 0, 1, 0, 1) is the most dispersed, leading therefore to the smallest power in the transmitting branch.

In practice, the full-width at half-maximum (FWHM) bandwidth of edge-emitting LED (ELED) light sources is approximately 50 nm. This coding bandwidth range is able to support M-sequence codes no longer than $N = 63$ when the wavelength grids are separated by 0.8 nm. On the other hand, the FWHM bandwidth of superluminescent diode (SLD) is approximately 90 nm, so wavelength grids separated by 0.8 nm cannot support an M-sequence code of $N = 127$. However, $N = 127$ can be supported when wavelength grids are separated by 0.4 nm.

In the following, SIR performance is evaluated with and without flatness compensation under M-sequence coding of length $N = 63$ on ELED light sources of FWHM$= 50$ nm and under M-sequence coding of length $N = 127$ on SLD light sources of FWHM$= 90$ nm.

Fig. 4 depicts the source flatness effect by comparing SIR performances for uncompensated and the compensated cases under M-sequence coding of length $N = 63$ on ELED light sources of FWHM$= 50$ nm. The coding region is chosen for a central band of $\lambda_1 = 1525.2$ nm $\sim \lambda_{63} = 1574.8$ nm, while compensating areas of $\lambda_{c33} = 1500.4$ nm $\sim \lambda_{c63} = 1524.4$ nm and $\lambda_{c1} = 1575.6$ nm $\sim \lambda_{c32} = 1600.4$ nm in the Gaussian

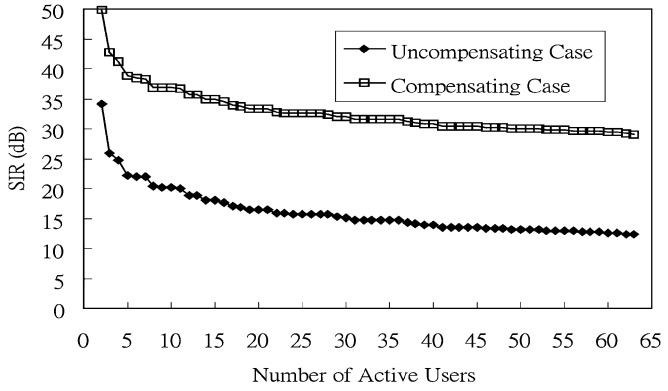

Fig. 4. SIR performance with and without source flatness compensation for code length $N = 63$, ELED light source, FWHM= 50 nm.

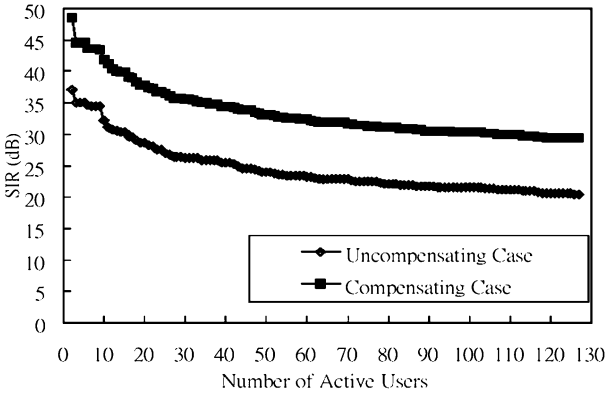

Fig. 5. SIR performance with and without source flatness compensation, code length $N = 127$, SLD light source of FWHM= 90 nm.

skirts are taken to examine the effects of source flatness compensation. Each spectral chip is separated by 0.8 nm at both the coding and the compensating regions. The coding-chips and the compensating-chips can then be one-to-one united to represent a FBG chip element of the signature code. As seen in Fig. 4, SIR performance under M-sequence codes of length $N = 63$ shows the source flatness compensated case is superior to the uncompensated case by ∼17 dB.

Fig. 5 depicts the source flatness effect by comparing SIR performances for uncompensated and compensated cases under SLD source of FWHM= 90 nm. The coding region is chosen at a central band of $\lambda_1 = 1524.8$ nm $\sim \lambda_{127} = 1575.2$ nm, while compensating areas of $\lambda_{c65} = 1480$ nm $\sim \lambda_{c127} = 1504.8$ nm and $\lambda_{c1} = 1595.2$ nm $\sim \lambda_{c64} = 1620.4$ nm in the Gaussian skirts are taken to examine the effects of source flatness compensation. Each spectral chip is separated by 0.4 nm at both coding and compensating regions. As seen in Fig. 5, SIR performance under M-sequence codes of length $N = 127$ shows the compensated case superior by ∼10 dB.

With the proposed source flatness compensation scheme, chips' power variation reduces to ∼7% and 9%, respectively, for the ELED in Fig. 4 and the SLD in Fig. 5. However, without source flatness compensation, the coding chips in the central Gaussian region have 50% and 20% variation, respectively. It should be noted that the data presented here are a simulation using ideal (true) Gaussian source spectrum. Under such ideal conditions, flatness compensation is achieved only when the coding bandwidth is fully contained in the FWHM of the source and the compensation chips are taken from the skirt region directly beside the central Gaussian profile, not from the far-end tails of the spectral distribution.

The traditional source equalization schemes [9], [10] and Nguyen's compensation scheme [11] all reduce MAI through the use of chip power equalization. The proposed SFC scheme does this also. Both Nguyen's system and SFC are superior to the source equalization schemes because of increased number of chips available from the same spectrum. SFC has an advantage over Nguyen's scheme because of the use of ITU-standard and easily manufactured FBGs. Thus, SFC has been shown theoretically to be a viable and possibly superior alternative to the various traditional methods for MAI reduction of spectral amplitude coding type of FO-CDMA networks.

VI. Conclusion

A novel source flatness compensation method has been presented to reduce multiple-access interference in FBG-based optical CDMA networks. In order to obtain chips of equal power from a broad-band source with an unequal power spectrum, the proposed method supplies additional power to the lower power chips through common low-cost FBGs. This additional power comes from the "skirt area" power of the source, power that is unused in traditional methods. Although the proposed compensation scheme uses more FBGs to represent a chip than conventional schemes, simulated results show improved SIR in the range of ∼17 dB in Fig. 4 and ∼10 dB in Fig. 5.

With the proposed FO-CDMA coder/compensator and decompensator/decoder scheme, the MAI effects caused by nonflattened LED-like incoherent sources can be greatly suppressed. The compensating technique proposed in this paper therefore allows every user to successfully retrieve information data bits delivered from the transmitter. It is concluded that the inherent nonideal factors causing MAIs in fiber-optic CDMA systems can be greatly improved by the proposed flatness compensation method.

References

[1] J. A. Salehi, A. M. Weiner, and J. P. Heritage, "Coherent ultrashort light pulse code-division multiple-access communication systems," *J. Lightwave Technol.*, vol. 8, pp. 478–491, Mar. 1990.

[2] R. A. Griffin, D. D. Sampson, and D. A. Jackson, "Coherence coding for photonic code- division multiple access networks," *J. Lightwave Technol.*, vol. 13, pp. 1826–1837, Sept. 1995.

[3] L. R. Chen, S. D. Benjamin, P. W. E. Smith, and J. E. Sipe, "Applications of ultrashort pulse propagation in Bragg gratings for wavelength division multiplexing and code division multiple access," *IEEE J. Quantum Electron.*, vol. 34, pp. 2117–2129, Nov. 1998.

[4] A. Grunnet-Jepsen, A. Johnson, E. Maniloff, T. Mossberg, M. Munroe, and J. Sweetser, "Spectral phase encoding and decoding using fiber Bragg gratings," in *OFC/IOOC'99 Tech. Dig. PD33/1-PD33/3*, Feb. 21–26, 1999.

[5] H. Fathallah, L. A. Rusch, and S. LaRochelle, "Passive optical fast frequency-hop CDMA communications system," *J. Lightwave Technol.*, vol. 17, pp. 397–405, Mar. 1999.

[6] J. F. Huang and D. Z. Hsu, "Fiber-Grating-Based optical CDMA spectral coding with nearly orthogonal M-sequence codes," *IEEE Photon. Technol. Lett.*, vol. 12, pp. 1252–1254, Sept. 2000.

[7] J. F. Huang and C. C. Yang, "Reductions of multiple-access interference in fiber-grating- based optical CDMA network," *IEEE Trans. Commun.*, vol. 50, pp. 1680–1687, Oct. 2002.

[8] Z. Wei, H. M. H. Shalaby, and H. Ghafouri-Shiraz, "Modified quadratic congruence codes for fiber Bragg-grating-based spectral-amplitude-coding optical CDMA systems," *J. Lightwave Technol.*, vol. 19, pp. 1274–1281, Sept. 2001.
[9] J. E. Baran, G. Joyce, R. Olshansky, D. A. Smith, and S. F. Su, "Gain equalization multiwavelength lightwave systems using acoustooptic tunable filters," *IEEE Photon. Technol. Lett.*, vol. 4, pp. 269–271, Mar. 1992.
[10] P. M. J. Schiffer, C. R. Doerr, L. W. Stulz, M. A. Cappuzzo, E. J. Laskowski, A. Paumescu, L. T. Gomez, and J. V. Gates, "Smart dynamic wavelength equalizer based on an integrated planar optical circuit for use in the 1550-nm region," *IEEE Photon. Technol. Lett.*, vol. 11, pp. 1150–1152, 1999.
[11] L. Nguyen, T. Dennis, B. Aazhang, and J. F. Young, "Experimental demonstration of bipolar codes for optical spectral amplitude CDMA communication," *J. Lightwave Technol.*, vol. 15, pp. 1647–1653, Sept. 1997.
[12] M. Kavehrad and D. Zaccarin, "Optical code-division-multiplexed systems based on spectral encoding of noncoherent sources," *J. Lightwave Technol.*, vol. 13, pp. 534–545, Mar. 1995.

Jen-Fa Huang received the M.A.Sc. and Ph.D. degrees from the Department of Electrical Engineering, University of Ottawa, ON, Canada, in 1981 and 1985, respectively.

He was previously with the Optical Communication Laboratories, MPB Technologies, Montreal, QC, Canada, working on the TAT-9 transatlantic undersea lightwave transmission project. Since 1991, he has been with the Department of Electrical Engineering, National Cheng Kung University, Taiwan, where he is currently a conjunct Professor of the Institute of Computer and Communication Engineering and the Institute of Electro-Optical Science and Engineering. His research interests are mainly in the areas of optical communications, all-optical data networking, and passive optical devices.

Chen-Mu Tsai was born in Tainan, Taiwan, in October 1974. He received the B.S. degree from the Department of Electronic Engineering, National Taiwan University of Science and Technology, in 1999. He is currently working toward the Ph.D. degree in fiber-optic communications with the Department of Electrical Engineering, National Cheng Kung University, Taiwan.

His major interests are in multi-user optical communications and in dense-wavelength-division-multiplexing (DWDM) data networks.

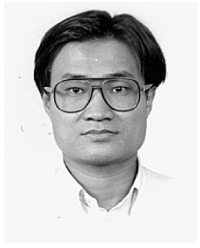

Yu-Lung Lo received the B.S. degree from the National Cheng Kung University, Taiwan, in 1985, and the M.S. and Ph.D. degrees in mechanical engineering from the Smart Materials and Structures Research Center, University of Maryland, College Park, in 1992 and 1995, respectively.

After graduation, he joined the Opto-Electronics & Systems Laboratories of the Industrial Technology Research Institute (ITRI), working on fiber-optic smart structures. He has been a Member of the Faculty of the Mechanical Engineering Department at National Cheng Kung University since 1996. Currently, he is Full Professor. His research interests are in the areas of optical passive components in telecom, fiber-optic sensors, optical techniques in precision measurements, electronic packaging, and microelectromechanical systems (MEMS). He has authored over 50 technical publications and filed several patent disclosures.

Dr. Lo is a Member of the SPIE and the SEM.